CrystEngComm

RSC Publishing

PAPER

View Article Online
View Journal | View Issue

Cite this: *CrystEngComm*, 2013, **15**, 9530

Two new polar coordination polymers with diamond networks: interpenetration and thermal phase transition†

Xiao-Lin Qi, Chi Zhang, Bao-Ying Wang, Wei Xue, Chun-Ting He, Si-Yang Liu, Wei-Xiong Zhang* and Xiao-Ming Chen*

Received 12th June 2013,
Accepted 23rd July 2013

DOI: 10.1039/c3ce41111g

www.rsc.org/crystengcomm

Two new polar coordination polymers, $[Cu(Hmpc)_2]$ (**1**) and $[Cu_2(mpc)_2(DMA)]$ (**2**), were synthesized by solvothermal reactions of a ligand 3,5-dimethyl-1*H*-pyrazole-4-carboxylic acid (H_2mpc) with $Cu(NO_3)_2$. Single-crystal X-ray analysis reveals that **1** crystallizes in the orthorhombic, polar space group *Fdd*2. Each square-planar coordinated Cu^{2+} ion is linked to four adjacent Cu^{2+} ions by mono-deprotonated $Hmpc^-$ ligands, resulting in a severely distorted 4-connected diamond network, inside which the methyl groups of the ligands are densely packed. In **2**, non-centrosymmetric binuclear Cu^{2+} units serve as 4-connecting nodes, forming a non-porous polar structure consisting of 2-fold-interpenetrated diamond networks. A thermal structural phase transition was detected in **2** at around 323 K. At 298 K, **2** crystallizes in the tetragonal chiral space group $P4_1$ (**2α**), with a = 10.9931 (6) Å, c = 18.0850(9) Å, and Z = 4, whereas at a higher temperature (438 K) it is transferred to the tetragonal non-centrosymmetric space group $P4_2nm$ (**2β**), with a = 10.9857(5) Å, c = 9.1031(9) Å, and Z = 2. By repeating *in situ* single-crystal X-ray diffraction, this phase transition was found to be reversible between a non-twinning non-centrosymmetric crystal (**2β**) and a racemic-twinning chiral crystal (**2α**). The symmetry of the diamond network was increased from C_1 to D_{2d} in the heating process, so that two fold interpenetrated networks become strictly parallel along the *c*-axis at about 323 K, and the *c*-axis was halved in **2β**. At the same time, 2-fold disordered coordinated DMA molecules in **2α** were found to be 8-fold disordered in **2β**. According to *aizu* notation, **2** can be classified as 4*mmF*4 species, which are potentially secondary ferroic.

Introduction

Coordination polymers (CPs) have attracted considerable attention in the past decade primarily because of their aesthetic and varied structures, chemical and physical properties, as well as structural responses to external stimuli. Responsive behaviours of CPs toward temperature,[1] light,[2] magnetic field,[3] and electronic field[4] have been well known, which may spark a broad spectrum of interest in CPs as functional materials, such as thermal expansion materials, magnetic materials for information storage, as well as ferroelectric materials used as ferroelectric random access memories.[1,3–5]

Although polycarboxylate ligands can bridge rigid metal clusters as nodes into CPs with structurally predictable frameworks, the variable coordination geometry of the carboxylate can easily link single metal ions in different modes into frameworks of unpredictable topologies.[6] In contrast, polypyridines can afford more predictable coordination modes for single metal ions in rational design and assembly of thermodynamically favoured architectures. However, neutral frameworks cannot be furnished using only neutral pyridine-like ligands and metal ions due to the charge balance requirement.[7] Combining the advantages of both carboxylate and pyridyl groups, anionic and bifunctional pyridyl–carboxylate ligands are a good approach to construct neutral CPs.[8] Azole ligands with strong coordination capability and predictable coordination behaviour make metal azolate frameworks of great interest for some unique properties in sorption, separation and so on.[9] Among several kinds of azolates, pyrazolates adopt a similar bidentate bridging coordination mode as carboxylates.[10] In particular, pyrazolates have higher pK_a values and can be expected to form more stable CPs than carboxylates. A ligand containing both pyrazolate and carboxylate

MOE Key Laboratory of Bioinorganic and Synthetic Chemistry, State Key Laboratory of Optoelectronic Materials and Technologies, School of Chemistry and Chemical Engineering, Sun Yat-Sen University, Guangzhou 510275, China.
E-mail: zhangwx6@mail.sysu.edu.cn, cxm@mail.sysu.edu.cn;
Fax: +86-20-84112245; Tel: +86-20-84115358

† Electronic supplementary information (ESI) available: Thermogravimetry curves, variable-temperature powder X-ray diffraction patterns, and differential scanning calorimeter curves. CCDC 952286–952292. For ESI and crystallographic data in CIF or other electronic format see DOI: 10.1039/c3ce41111g

groups is a good candidate to construct neutral CPs with advantages of both pyrazole and carboxylate donors.[11] On the other hand, the asymmetric distribution of functional groups may result in polar structures,[11d] and even chiral structures.[12]

Herein we choose a less exploited ligand, 3,5-dimethyl-1*H*-pyrazole-4-carboxylic acid (H_2mpc) to construct polar CPs. Two new polar diamond CPs [Cu(Hmpc)$_2$] (**1**) and [Cu_2(mpc)$_2$(DMA)] (**2**) were obtained by altering the reaction conditions. **1** is a non-interpenetrated densely packed network and **2** is a 2-fold interpenetrated network constructed with a binuclear unit. Interestingly, a reversible phase transition caused by the coordination geometric distortion of the metal ions was uncovered for **2**.

Experimental section

General information

The ligand H_2mpc was synthesized according to the literature method.[13] Other reagents and solvents were commercially available and were used without further purification. Elemental analyses (C, H, N) were performed with a Vario EL elemental analyzer. Powder X-ray diffraction (PXRD) patterns were recorded on a Bruker D8 ADVANCE X-ray powder diffractometer (Cu Kα). Thermogravimetric analyses (TGA) were performed with a TA Q50 instrument. Each sample was heated with a heating rate of 5.0 °C min^{-1} under N_2 atmosphere. Differential scanning calorimetery was performed using a NETZSCH DSC 204F1. The magnetic susceptibility data of random orientation powder samples were collected in the temperature range of 2.0–300 K with Quantum Design MPMS XL-7 SQUID magnetometer. All data were corrected for the diamagnetism of each sample (estimated with Pascal's constants), as well as for the temperature-independent paramagnetism (60×10^{-6} cm^3 mol^{-1} per Cu^{2+} ion).

X-ray crystallography

Diffraction intensities were collected on a Bruker Apex CCD diffractometer with graphite-monochromated Mo Kα radiation or an Oxford Gemini S Ultra CCD diffractometer using mirror-monochromated Cu Kα radiation or a Rigaku R-AXIS SPIDER IP diffractometer with Mo Kα radiation. The measurement temperatures were controlled by a dry nitrogen open flow using a Rigaku Gas Flow GN2 apparatus with temperature fluctuation less than 0.1 K, and corrected by a thermal couple at the crystal position. Absorption corrections were applied by using multi-scan program SADABS.[14] The structures were solved with direct methods and refined with a full-matrix least-squares technique with the SHELXTL program package.[15] Anisotropic thermal parameters were applied to all non-hydrogen atoms. All the hydrogen atoms were generated geometrically. The disordered terminal molecules in **2α** and **2β** were subjected to geometric restrains during the refinement. Twinning law (0 −1 0 −1 0 0 0 0 1) was used during the structure refinement for **2α**.

Synthesis

[Cu(Hmpc)$_2$] (1). A mixture of $Cu(NO_3)_2 \cdot 3H_2O$ (0.1 mmol, 0.030 g), H_2mpc (0.2 mmol, 0.028 g), and H_2O (6 mL) was sealed in a 12 mL Teflon-lined reactor, heated at 80 °C for 3 days and cooled to room temperature at a rate of 5 °C h^{-1}. Violet, bar-like crystals of **1** were collected by filtration (yield 40% on the basis of Cu). Elemental analysis calculated: C, 42.17%, H, 4.13%, N, 16.39%. Found: C, 41.96%, H, 4.17%, N, 16.64%.

[Cu_2(mpc)$_2$(DMA)] (2). The mixture of $Cu(NO_3)_2 \cdot 3H_2O$ (0.2 mmol), H_2mpc (0.2 mmol), DMA (2 mL), and MeOH (6 mL) was sealed in a 12 mL Teflon-lined reactor, heated at 110 °C for 3 days, cooled by 5 °C h^{-1} to room temperature and blue block crystals of **2** were collected by filtration (yield 70% on the basis of Cu). Elemental analysis calculated: C, 39.18%, H, 4.32%, N, 14.28%. Found: C, 38.61%, H, 4.38%, N, 14.24%.

Results and discussion

Synthesis

Solvothermal reaction of $Cu(NO_3)_2$ and H_2mpc gave crystals of [Cu(Hmpc)$_2$] (**1**) in H_2O and [Cu_2(mpc)$_2$(DMA)] (**2**) in mixed methanol–*N*,*N*-dimethylacetamide (DMA) solvent, respectively. The reactions were found independent on the molar ratio of reagents H_2mpc/$Cu(NO_3)_2$ in the range of 0.2–5. Apparently, DMA plays a key role in the formation of **2**, not only in the deprotonation of H_2mpc, but also participating in coordination and the formation of binuclear metal centre, leading to a higher yield for **2**.

Crystal structures

Single-crystal X-ray structural analysis at 150 K indicates that **1** crystallizes in the orthorhombic, non-centrosymmetric space group *Fdd*2, which belongs to the polar point group *mm*2. As shown in Fig. 1a, its asymmetric unit consists of half a Cu^{2+} ion and one $Hmpc^-$ ligand. Each Cu^{2+} ion locates at a crystallographic C_2 axis, adopting a square-planar geometry *via* coordination with two pyrazyl nitrogen atoms and two carboxylate oxygen atoms [Cu1–N1 2.001(2) Å, Cu1–O2 1.924(2) Å] in a *trans* fashion from four different $Hmpc^-$ entities. The N and O atoms deviate from the CuN_2O_2 least-square plane by 0.273(3) Å and 0.222(3) Å, respectively, indicating a slightly distorted square-planar coordination geometry. Each $Hmpc^-$ uses a carboxylate oxygen atom and a pyrazole nitrogen atom to link two Cu^{2+} ions. It can be concluded from the pK_a values of the carboxyl and pyrazole groups that the remaining proton is attached on the uncoordinated nitrogen atom of the pyrazole group. As shown in Fig. 1a and 1b, each N–H group forms a hydrogen bond [N1···O1D 2.747(4) Å, N1–H···O1D 153(5)° symmetry code of D: −0.25 + *x*, 0.25 − *y*, 0.75 + *z*] with the uncoordinated oxygen atom of a carboxylate group coordinated with an adjacent Cu^{2+} ion. By regarding the square-planar coordinated Cu^{2+} ions as 4-connecting nodes, as shown in Fig. 1c and 1d, the extended coordination network of **1** can be simplified as a severely distorted diamond network with a node-to-node

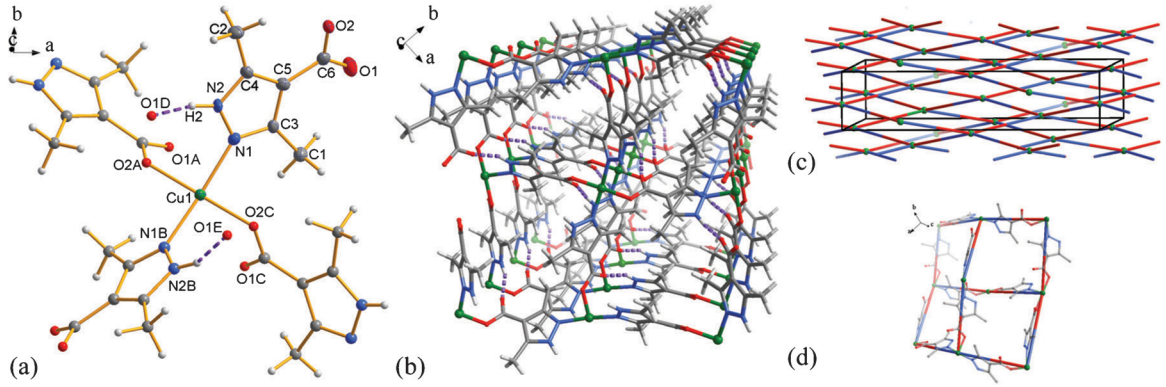

Fig. 1 (a) ORTEP plot [50% probability ellipsoids, (A) −0.25 + *x*, 0.25 − *y*, −0.25 + *z*; (B) −*x*, −*y*, *z*; (C) 0.25 − *x*, −0.25 + *y*, 0.25 − *z*; (D) −0.25 + *x*, 0.25 − *y*, 0.75 + *z*; (E) −0.25 − *x*, 0.25 + *y*, 0.75 + *z*] of the coordination environment in **1**, (b) diamond network of **1** with methyl groups filling in the cage, hydrogen bonds denoted as purple dashed lines and (c) simplified framework topology of **1**, (d) an isolated adamantine cage of **1**, hydrogen atoms are omitted for clarity.

Table 1 Summary of the crystal data and structure refinements for **1**, **2α** and **2β**

	1	**2α**	**2β**
Formula	$[Cu(Hmpc)_2]$ $C_{12}H_{14}CuN_4O_4$	$[Cu_2(mpc)_2(DMA)]$ $C_{16}H_{21}Cu_2N_5O_5$	$[Cu_2(mpc)_2(DMA)]$ $C_{16}H_{21}Cu_2N_5O_5$
Formula weight	341.81	490.46	490.46
Crystal system	Orthorhombic	Tetragonal	Tetragonal
Space group	*Fdd*2	$P4_1$	$P4_2nm$
a/Å	22.638(2)	10.9931(5)	10.9857(5)
b/Å	23.917(2)	10.9931(5)	10.9857(5)
c/Å	5.1656(4)	18.0850(9)	9.1031(9)
V/Å^3	2796.8(4)	2185.5(2)	1098.6(1)
Z	8	4	2
D_c (g cm^{-3})	1.624	1.491	1.483
μ (mm^{-1})	1.583	1.980	1.969
T/K	150	298	438
R_1	0.0327/0.0335	0.0316/0.0325	0.0271/0.0281
wR_2	0.0806/0.0816	0.0836/0.0849	0.0698/0.0706
GOF	1.051	1.010	1.027
$\Delta\rho$/e Å^3	0.631/−0.433	0.450/−0.334	0.209/−0.275
Flack	−0.01(2)	—	0.02(1)
BASF	—	0.50	—

separation, or the distance between adjacent Cu^{2+} ions, of 8.3336(5) Å. As the methyl groups of ligands are densely packed inside the framework, no solvent accessible volume is found in **1**.

At 298 K, single-crystal X-ray analysis reveals that **2** crystallizes in the tetragonal, chiral space group $P4_1$ (**2α** phase), containing two Cu^{2+} ions, two mpc^{2-} ligands and a coordinated DMA molecule in the asymmetric unit (Table 1). As shown in Fig. 2a, each Cu^{2+} ion adopts a square-pyramidal coordination geometry, with two nitrogen atoms from two mpc^{2-} ligands [1.944(5)–1.961(6) Å] and a chelating carboxylate from the third mpc^{2-} [1.991(5)–2.025(5) Å] in a *cis* N_2O_2 fashion on the basal plane, as well as a carbonyl oxygen (O5) from the DMA molecule on the apical position [Cu–O 2.298(3) and 2.262(3) Å]. The CuN_2O_2 basal planes of the square-pyramidal coordination environments are almost coplanar with a τ value of 0.012 for both Cu^{2+} ions,[16] as the atom with the largest deviation is N3 0.121(6) Å for Cu1 [Cu1 0.0043(5) Å, O4 0.079(5) Å, O3 0.093(5) Å, N1 0.114(5) Å] and N2 0.146(5) Å for Cu2 [Cu2 0.0076(6) Å, O2 0.061(4) Å, N4 0.129(5) Å, O1 0.129(5) Å], respectively. Each ligand coordinates to three Cu^{2+} ions through the *exo*-bidentate pyrazolate (pz) and chelating carboxylate groups, forming a 4-connected binuclear $Cu_2(pz)_2(COO)_2(DMA)$ unit. The intradimer Cu···Cu separation

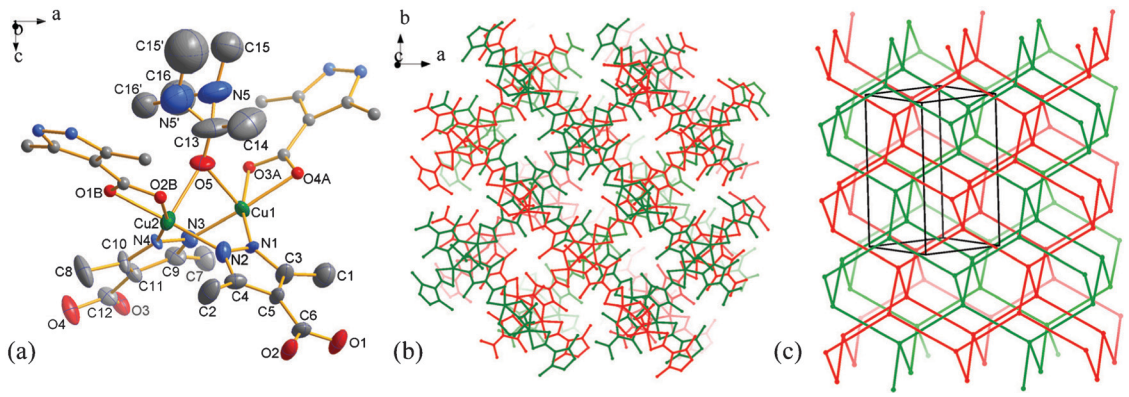

Fig. 2 (a) ORTEP plot [50% probability ellipsoids, (A) *y*, 1 − *x*, −0.25 + *z*; (B) −1 + *y*, 2 − *x*, −0.25 + *z*; hydrogen atoms are omitted for clarity] of the coordination environment in **2**, (b) diamond network and (c) simplified framework topology of **2**.

of 3.249(1) Å in 2α is relatively short in similar binuclear $Cu_2(pz)_2$ units (3.2–4.5 Å).[11d,17] The two pyrazolate moieties of the dinuclear unit form a dihedral angle of 71.5(2)°, while that of the two carboxylate groups is 73.8(4)°, which suggest that the binuclear unit is only slightly distorted from a regular tetrahedral geometry. Simplifying the Cu1 and Cu2 as one point at the middle of them, the binuclear unit can be regarded as a 4-connected node and mpc^{2-} as a linker (Fig. S1, ESI†), and the coordination network extends into a diamond network (Fig. 2b and 2c), which is isostructural with the non-interpenetrated network $[Cu_2(dmcapz)_2(OH_2)]_n$.[11d] Compared with **1**, 2α has a longer node-to-node separation [8.9451(2) Å and 9.0440(2) Å] and a less distorted network, thus a larger extraframework space should be expected. Indeed, the single diamond network contains a large void so that another identical diamond network is found interpenetrated. This 2-fold interpenetration negates the porosity of each network, and the whole structure of 2α is non-porous. In addition, merohedal twinning together with racemic twinning, in which the BASF value remained around 0.5, was found in the crystal structure refinement for 2α, though we carefully chose several crystals with perfect appearance (*vide infra*).

Thermal stability

Thermal stability of **1** was studied by thermogravimetric analysis (TGA) and variable-temperature powder X-ray diffraction (VTPXRD) (Fig. S2 and S3, ESI†), revealing that **1** is stable up to 513 K (240 °C). The PXRD patterns did not show any changes before the collapse of framework, which corresponds well with the dense structure of **1** and implies no phase transition in **1** above room temperature (Fig. S4, ESI†).

To explore whether the coordinated DMA can be removed, TGA and variable-temperature single-crystal X-ray diffraction was performed on **2**. The TGA curve of **2** shows that there is no weight loss below 270 °C until decomposition, indicating that the coordinated DMA molecule cannot be removed before the collapse of framework (Fig. S5, ESI†).

Thermal phase transition of 2

The crystal structure of 2α is of much lower symmetry than the apparent symmetry of its coordination structure. As the phase transition behaviors of complexes have been well documented, in which the disorder counter ions of frameworks usually make the structural symmetry transform into a higher one in the heating process, we speculate the orientation of the coordinated DMA molecule might become more disordered so that a more symmetrical structure might exist at higher temperatures.[18] Therefore, VTPXRD were measured by heating the powder sample of 2α. As shown in Fig. 3, the intensities of several diffraction peaks (*e.g.* at 8.0°, 18.6°, 21.7°, 23.3°) in the 2θ range of 8–30° became weaker and disappeared when the sample was heated up to 370 K. This fact suggests a thermal phase transition occurs in the range of 320–370 K.

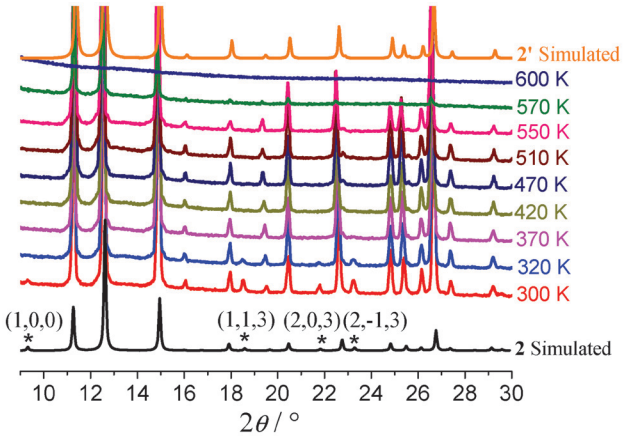

Fig. 3 VTPXRD patterns of **2**. The diffraction peaks diminishing at higher temperature are marked with asterisks.

The phase transition was further confirmed by the single-crystal X-ray analysis at 438 K, and a new phase (2β) was found to be in the tetragonal non-centrosymmetric space group $P4_2nm$ with higher symmetry than that of 2α. The *a*- and *b*-axes did not show obvious variation, while the *c*-axis reduced to almost half of that of 2α. 2β adopts a similar local coordination geometry and similar 3-D network to those of 2α (Fig. 4a–4c), and the number of its independent atoms in 2β became 1/4 of that in 2α. As a result, the 2-fold disordered DMA ligand locates at a C_{2v} axis, thus the orientations of its methyl/dimethylamino groups are 8-fold disordered in 2β (Fig. 4a). Interestingly, in this *in situ* variable-temperature measurement, the Flack value was close to zero, and no significant twinning was detected, indicating that the single-crystal changed from a racemic-twinning crystal with chiral structure to a non-twinning crystal with a non-centrosymmetric structure. To confirm this change in the phase transition procedure, we picked another crystal with perfect appearance and collected its single-crystal X-ray diffraction data twice at room and high temperatures, respectively, and a similar trend of Flack/BASF value was observed repeatedly (Table S1, ESI†). Although some phase transitions occurring in CPs,[19] especially in some ferroelectric ones,[4a,20] have been documented, reversible phase transitions between a racemic-twinning chiral structure and a non-twinning non-centrosymmetric structure were rarely reported.[21] According to *aizu* notation, which denotes the species by a symbol containing the point group of the prototype phase followed by the point group of the twinned phase,[22] the phase transition between 2α and 2β can be noted by 4*mmF*4, indicating that **2** is neither ferroelectric nor ferroelastic, but potentially ferrobielastic and ferroelastoelectric.[23]

In order to check whether another phase of **2** exists at a lower temperature, we collected the single-crystal diffraction data at 123 K, and obtained a tetragonal primitive cell by indexing the data. However, we failed to solve the structure, possibly because the network kept distorting and the crystallinity became worse at lower temperature. For figuring out the exact thermal expansion status in the structural transition, we determined unit-cell parameters of the same single

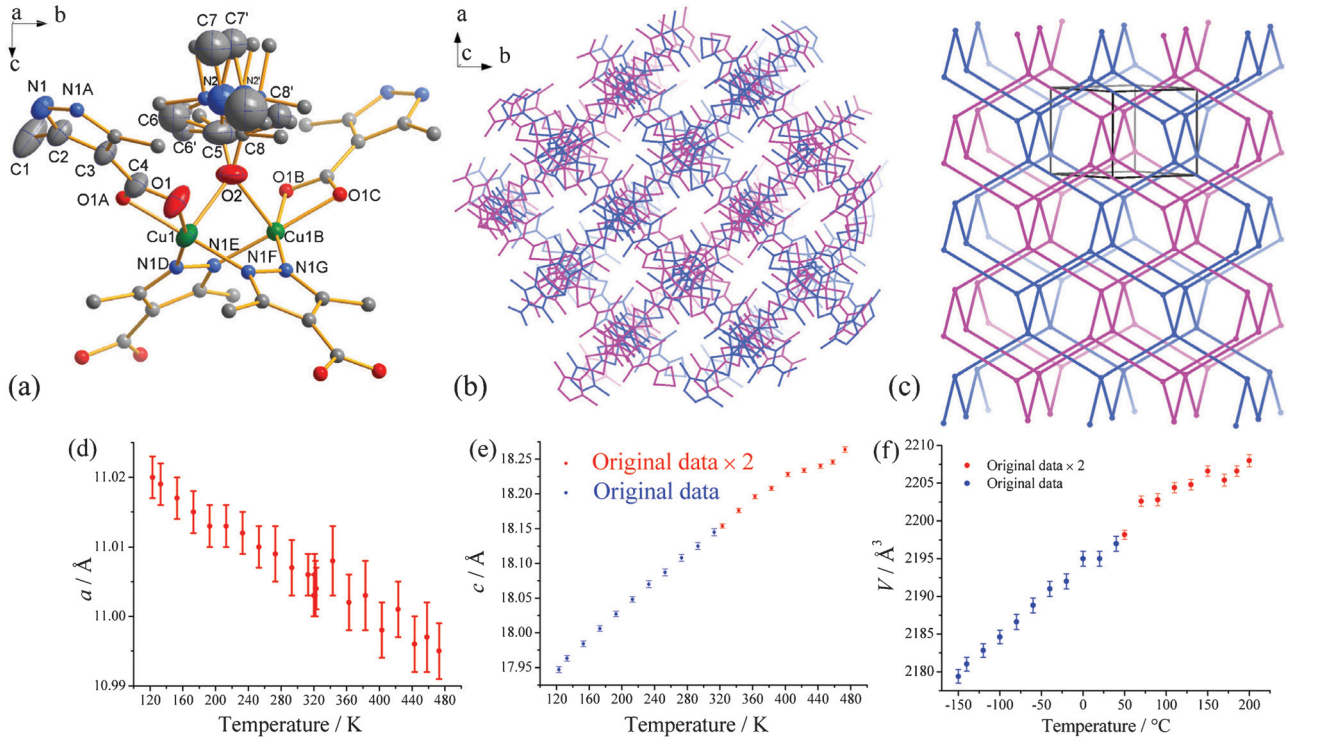

Fig. 4 (a) ORTEP plot [50% probability ellipsoids, (A) *x*, *y*, *z*; (B) −1 − *x*, −1 − *y*, *z*; (C) −1 − *y*, −1 − *x*, *z*; (D) 0.5 + *y*, −1.5 − *x*, 0.5 + *z*; (E) 0.5 + *x*, −1 − *y*, 0.5 + *z*; (F) −1.5 − *x*, 0.5 + *y*, 0.5 + *z*; (G) −1.5 − *y*, 0.5 + *x*, 0.5 + *z*; hydrogen atoms are omitted for clarity] of the coordination environment in **2β**, (b) diamond network and (c) simplified framework topology of **2β**, variable-temperature unit-cell parameters in the phase transition procedure between **2α** and **2β**. Temperature dependence of the lengths of (d) *a*-axis, (e) *c*-axis and (f) cell volume.

crystal at different temperatures (Fig. 4d–4f). From 123 K to 458 K, the unit-cell parameters show approximately linear changes. Above 323 K, the length of the *c*-axis abruptly halved, indicating occurrence of the phase transition. In order to compare the *c*-axes of the two phases, the *c*-axis length of **2β** phase is multiplied by 2 in Fig. 4e. The *c*-axis (thermal expansion coefficient = 7.4×10^{-6} K^{-1}) and unit-cell volume (thermal expansion coefficient = 6.8×10^{-6} K^{-1}) follow the law of thermal expansion and contraction, while the length of the *a*-axis (thermal expansion coefficient = -0.55×10^{-6} K^{-1}) reduces on increasing temperature (Fig. 4d–4f). The positive/negative thermal expansion coefficients of these cell axes are not significant compared with typical thermal expansion materials,[1] which indicates a weak thermal effect in this process so that no significant thermal abnormality was found in DSC measurements (Fig. S6, ESI†).

As shown in Fig. 5, by comparing coordination environments and networks of **2α** and **2β**, we can find that the coordination geometry of Cu^{2+} ions is distorted slightly during the phase transition procedure. In **2β**, the coordination geometry of Cu^{2+} ions is closer to an ideal square-pyramid with a τ value of 0, and the deviations of all the atoms from the CuN_2O_2 basal plane decrease slightly [Cu1 0.0131(4) Å, O1 0.089(3) Å, N1 0.113(3) Å]. The Cu···Cu separation in the binuclear unit slightly increases from 3.249(1) Å in **2α** to 3.2576(4) Å in **2β**. Two different node-to-node separations [8.9451(2) and 9.0440(2) Å] exist in **2α**, and they tend to be equal through lax distortion upon increasing temperature, and consequently become identical [9.0033(4) Å] at 323 K. Therefore, the length of linkers in each fold of the diamond networks of **2β** became equal, the interpenetrated networks are transformed to be strictly parallel along the *c*-axis, the *c*-axis is halved and additional symmetries are found (Fig. 4c). In short, the phase transition should be mainly ascribed to the slight distortion of the framework during which the absence of gain and loss of guest/coordinated molecules and the weak thermal effect during this structural transition enable the transition to be reversible. Moreover, when the structure is changed from **2β** to **2α**, the coordination structure distorted along two directions, that is why the racemic-twinning was detected in **2α** phase. In addition, as shown in Table 2 and Fig. 5c, we can find that, in the **2β** phase, the distances between adjacent nodes (O–A, O–B, O–C, O–D) slightly increase, while the angles ∠AOB and ∠COD slightly decrease, compared with those in the **2α**

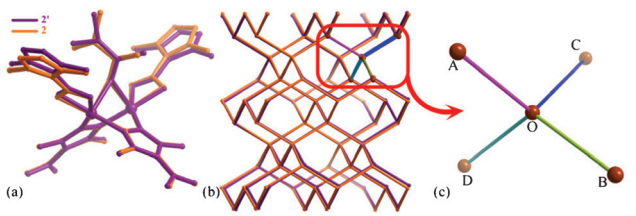

Fig. 5 Comparison of (a) coordination environments and (b) simplified networks between **2α** and **2β**. (c) Magnified node of the red rectangle in (b).

Table 2 Summary of the structure data of **2α** and **2β**

	2α	**2β**
Bond length of Cu–N (Å)	1.944(5), 1.961(6), 1.961(6), 1.967(5)	1.963(2)
Bond length of Cu–O (carboxylate) (Å)	1.991(5), 2.006(4), 2.014(6), 2.025(5)	2.010(2)
Bond length of Cu–O (DMA) (Å)	2.298(3), 2.262(3)	2.287(3)
Cu···Cu separation (Å)	3.249(1)	3.2576(4)
Deviation of least-square plane	Cu1 0.0043(5), O4 0.079(5), O3 0.093(5), N1 0.114(5), N3 0.121(6), Cu2 0.0076(6), O2 0.061(4), N4 0.129(5), O1 0.129(5), N2 0.146(5)	Cu1 0.0131(4), O1 0.089(3), N1 0.113(3)
Distance between adjacent nodes (Å)	8.9451(2), 9.0440(2)	9.0033(4)
∠COB, ∠COA, ∠AOD, ∠BOD (°)	104.8, 106.8, 104.5, 102.5	104.8
∠AOB, ∠COD (°)	119.6	119.3

phase, which corresponds to the negative thermal expansion of the *a*-axis, and the thermal expansion of the *c*-axis.

Magnetic studies

Magnetic measurements were performed on ground polycrystalline samples of **1** and **2** in a dc field of 5 kOe and 1 kOe, respectively. As shown in Fig. 6, a round peak was found in the χ_m *vs.* *T* plot at around 10 K for **1** and 140 K for **2**, respectively, indicating that antiferromagnetic interactions are dominant in both **1** and **2**. In **1**, each Cu^{2+} ion is linked to six neighboring Cu^{2+} ions, by four $Hmpc^-$ bridges with a Cu···Cu distance of 8.3336(5) Å and two hydrogen-bonded pyrazole–carboxylate bridges with Cu···Cu distance of 5.124(1) Å. Since these bridges should pass antiferromagnetic interactions with similar amplitudes, the molecular field approximation was employed for **1**, giving its magnetic susceptibility by eqn (1),

$$\chi_{cal} = \frac{Ng^2\mu_B^2 S(S+1)}{3kT - zJS(S+1)} \quad (1)$$

where, *N*, *β*, *g*, *k* and *T* are Avogadro number, Bohr magneton, *g*-factor, Boltzmann constant and temperature, respectively. *J* is the interaction parameter between two nearest neighboring Cu^{2+} ions, and $z = 6$, is the number of nearest neighbors around each Cu^{2+} ion. The data above 18 K were used to fit the eqn (1), affording $g = 2.07$ and $J = -6.2$ cm^{-1}. The *g* factor is slightly larger than the spin only value of 2.0, which might be caused by the distorted coordination geometry of Cu^{2+} ion.

For **2**, at low temperature region, χ increases again on cooling further, which is often observed for polymetallic compounds with a singlet ground state, *e.g.* the well-known compound $Cu_2(CH_3COO)_4(H_2O)_2$.[24] It is not intrinsic to the compound but is due to the presence of a very small amount of non-coupled species in the sample. In order to clarify the magnetic interactions, the data were analyzed by using a Heisenberg dimer model in the form of $\hat{H} = -JS_1S_2$ with $S_1 = S_2 = 1/2$, taking into account non-coupled impurity species (mole fraction, ρ), assumed to follow a Curie law:

$$\chi_{cal} = \frac{Ng^2\mu_B^2}{kT\left(e^{-J/kT}+3\right)}(1-\rho) + \rho\frac{Ng^2\mu_B^2 S(S+1)}{3kT} \quad (2)$$

The best fit of eqn (2) to the data was achieved with $g = 2.01$, $J = -159.0$ cm^{-1}, and $\rho = 0.0043$ for **2**. The obtained *J* value of -159.0 cm^{-1} is consistent with the typical values in the range of -140 to -270 cm^{-1} for similar binuclear $Cu_2(pz)_2$ compounds,[17a,b] and with the longer inter-metallic distance of 3.249(1) Å within binuclear units.

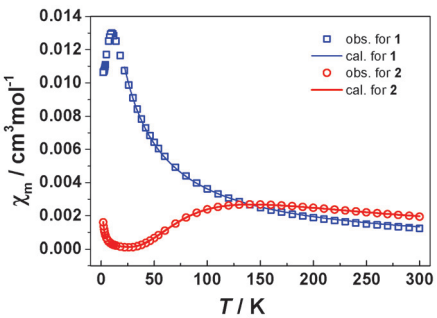

Fig. 6 The temperature dependence of magnetic susceptibility of **1** (□) and **2** (○) under a static field of 5 kOe and 1 kOe, respectively. The solid lines represent the best fitting curves (see the text).

Conclusions

In summary, two new polar CPs based on diamond networks with different interpenetration and nodes were synthesized with a non-symmetric ligand and copper(II) salt, by altering the reaction temperature and solvent. **1** consists of a non-interpenetrated densely packed network constructed with single metal-ion nodes, while **2** consists of 2-fold interpenetrated networks constructed with binuclear units. Due to the slight distortion of a single network, whose linker trends to be of the same length at higher temperature, a reversible temperature-induced phase transition at around 323 K was found in **2**. The *in situ* single-crystal X-ray analyses at 298 K and 438 K indicates that the transition occurs between a non-twinning non-symmetric structure in point group *4mm* and a racemic-twinning chiral structure in point group 4. More importantly, the results demonstrate that the unique flexibility of coordination bonds in CPs is beneficial to design new CPs with phase transition for ferroelectricity, multiferroicity, and liquid crystals.

Acknowledgements

This work was supported by the NSFC (21290173, 90922031, and 21121061), the 973 Project (2012CB821706), and NSF of Guangdong (S2012030006240). W.-X. Z. is grateful to SYSU for "100 Talents Program of SYSU" initial funding.

Notes and references

1 (*a*) A. L. Goodwin, M. Calleja, M. J. Conterio, M. T. Dove, J. S. O. Evans, D. A. Keen, L. Peters and M. G. Tucker, *Science*, 2008, **319**, 794; (*b*) Y. Wu, A. Kobayashi, G. J. Halder, V. K. Peterson, K. W. Chapman, N. Lock, P. D. Southon and C. J. Kepert, *Angew. Chem., Int. Ed.*, 2008, **47**, 8929.

2 (*a*) R. Lyndon, K. Konstas, B. P. Ladewig, P. D. Southon, P. C. J. Kepert and M. R. Hill, *Angew. Chem., Int. Ed.*, 2013, **52**, 3695; (*b*) G. K. Kole and J. J. Vittal, *Chem. Soc. Rev.*, 2013, **42**, 1755.

3 (*a*) M. Kurmoo, *Chem. Soc. Rev.*, 2009, **38**, 1353; (*b*) S. Takaishi, N. Ishihara, K. Kubo, K. Katoh, B. K. Breedlove, H. Miyasaka and M. Yamashita, *Inorg. Chem.*, 2011, **50**, 6405.

4 (*a*) T. Hang, W. Zhang, H.-Y. Ye and R.-G. Xiong, *Chem. Soc. Rev.*, 2011, **40**, 3577; (*b*) W. Zhang and R.-G. Xiong, *Chem. Rev.*, 2012, **112**, 1163.

5 H.-X. Zhao, X.-J. Kong, H. Li, Y.-C. Jin, L.-S. Long, X. C. Zeng, R.-B. Huang and L.-S. Zheng, *Proc. Natl. Acad. Sci. U. S. A.*, 2011, **108**, 3481.

6 (*a*) H. Li, M. Eddaoudi, M. O'Keeffe and O. M. Yaghi, *Nature*, 1999, **402**, 276; (*b*) G. Ferey, C. Mellot-Draznieks, C. Serre, F. Millange, J. Dutour, S. Surble and I. Margiolaki, *Science*, 2005, **309**, 2040.

7 M. Kondo, M. Shimamura, S.-i. Noro, Y. Kimura, K. Uemura and S. Kitagawa, *J. Solid State Chem.*, 2000, **152**, 113.

8 (*a*) O. R. Evans, R.-G. Xiong, Z. Wang, G. K. Wong and W. Lin, *Angew. Chem., Int. Ed.*, 1999, **38**, 536; (*b*) Y.-B. Zhang, H.-L. Zhou, R.-B. Lin, C. Zhang, J.-B. Lin, J.-P. Zhang and X.-M. Chen, *Nat. Commun.*, 2012, **3**, 642; (*c*) Y.-S. Wei, K.-J. Chen, P.-Q. Liao, B.-Y. Zhu, R.-B. Lin, H.-L. Zhou, B.-Y. Wang, W. Xue, J.-P. Zhang and X.-M. Chen, *Chem. Sci.*, 2013, **4**, 1539.

9 (*a*) J.-P. Zhang, Y.-B. Zhang, J.-B. Lin and X.-M. Chen, *Chem. Rev.*, 2012, **112**, 1001; (*b*) J.-P. Zhang, X.-C. Huang and X.-M. Chen, *Chem. Soc. Rev.*, 2009, **38**, 2385; (*c*) J.-P. Zhang and X.-M. Chen, *J. Am. Chem. Soc.*, 2008, **130**, 6010; (*d*) J.-P. Zhang and X.-M. Chen, *J. Am. Chem. Soc.*, 2009, **131**, 5516; (*e*) D. Marquardt, Z. Xie, A. Taubert, R. Thomann and C. Janiak, *Dalton Trans.*, 2011, **40**, 8290; (*f*) I. Boldog, K. V. Domasevitch, I. A. Baburin, H. Ott, B. Gil-Hernandez, J. Sanchiz and C. Janiak, *CrystEngComm*, 2013, **15**, 1235.

10 (*a*) F. Salles, G. Maurin, C. Serre, P. L. Llewellyn, C. Knöfel, H. J. Choi, Y. Filinchuk, L. Oliviero, A. Vimont, J. R. Long and G. Férey, *J. Am. Chem. Soc.*, 2010, **132**, 13782; (*b*) M. Tonigold, Y. Lu, B. Bredenkötter, B. Rieger, S. Bahnmüller, J. Hitzbleck, G. Langstein and D. Volkmer, *Angew. Chem., Int. Ed.*, 2009, **48**, 7546.

11 (*a*) C. Montoro, F. Linares, E. Q. Procopio, I. Senkovska, S. Kaskel, S. Galli, N. Masciocchi, E. Barea and J. A. R. Navarro, *J. Am. Chem. Soc.*, 2011, **133**, 11888; (*b*) D. J. Tranchemontagne, K. S. Park, H. Furukawa, J. Eckert, C. B. Knobler and O. M. Yaghi, *J. Phys. Chem. C*, 2012, **116**, 13143; (*c*) E. Q. Procopio, F. Linares, C. Montoro, V. Colombo, A. Maspero, E. Barea and J. A. R. Navarro, *Angew. Chem., Int. Ed.*, 2010, **49**, 7308; (*d*) E. Q. Procopio, T. Fukushima, E. Barea, J. A. R. Navarro, S. Horike and S. Kitagawa, *Chem.–Eur. J.*, 2012, **18**, 13117.

12 S. C. Sahoo, T. Kundu and R. Banerjee, *J. Am. Chem. Soc.*, 2011, **133**, 17950.

13 J. Chen, H.-T. Xi, X.-Q. Zhang, Q. Meng, Y. Jiang and X.-Q. Zhang, *Fine Chem.*, 2007, **24**, 199.

14 *SADABS, SMART and SAINT*, Bruker AXS Inc., Madison, WI, 2002.

15 G. M. Sheldrick, *SHELXL-97, Program for the Refinement of Crystal Structures*, University of Göttingen, Göttingen, Germany, 1997.

16 A. W. Addison, T. N. Rao, J. Reedijk, J. van Rijn and G. C. Verschoor, *J. Chem. Soc., Dalton Trans.*, 1984, 1349.

17 (*a*) H. Matsushima, H. Hamada, K. Watanabe, M. Koikawa and T. Tokii, *J. Chem. Soc., Dalton Trans.*, 1999, 971; (*b*) E. Spodine, A. M. Atria, J. Valenzuela, J. Jalocha, J. Manzur, A. M. García, M. T. Garland, O. Peña and J.-Y. Saillard, *J. Chem. Soc., Dalton Trans.*, 1999, 3029; (*c*) O. A. Bondar, L. V. Lukashuk, A. B. Lysenko, H. Krautscheid, E. B. Rusanov, A. N. Chernega and K. V. Domasevitch, *CrystEngComm*, 2008, **10**, 1216; (*d*) S.-Y. Yu, H.-P. Huang, S.-H. Li, Q. Jiao, Y.-Z. Li, B. Wu, Y. Sei, K. Yamaguchi, Y.-J. Pan and H.-W. Ma, *Inorg. Chem.*, 2005, **44**, 9471.

18 (*a*) A. Piecha, M. Weclawik, A. Gagor, R. Jakubas and W. Medycki, *CrystEngComm*, 2013, **15**, 5633; (*b*) D.-W. Fu, H.-L. Cai, S.-H. Li, Q. Ye, L. Zhou, W. Zhang, Y. Zhang, F. Deng and R.-G. Xiong, *Phys. Rev. Lett.*, 2013, **110**; (*c*) D. W. Fu, H. L. Cai, Y. Liu, Q. Ye, W. Zhang, Y. Zhang, X. Y. Chen, G. Giovannetti, M. Capone, J. Li and R. G. Xiong, *Science*, 2013, **339**, 425; (*d*) M. Szafranski and M. Jarek, *J. Phys. Chem. B*, 2008, **112**, 3101.

19 (*a*) W. X. C. Oliveira, M. A. Ribeiro, C. B. Pinheiro, W. C. Nunes, M. Julve, Y. Journaux, H. O. Stumpf and C. L. M. Pereira, *Eur. J. Inorg. Chem.*, 2012, 5685; (*b*) G.-C. Xu, X.-M. Ma, L. Zhang, Z.-M. Wang and S. Gao, *J. Am. Chem. Soc.*, 2010, **132**, 9588.

20 Z. Sun, J. Luo, T. Chen, L. Li, R.-G. Xiong, M.-L. Tong and M. Hong, *Adv. Funct. Mater.*, 2012, **22**, 4855.

21 Z. Sun, T. Chen, J. Luo and M. Hong, *Angew. Chem., Int. Ed.*, 2012, **51**, 3871.

22 K. Aizu, *Phys. Rev. B: Solid State*, 1970, **2**, 754.

23 (*a*) R. E. Newnham, *Am. Mineral.*, 1974, **59**, 906; (*b*) B. O. Hildmann and T. Hahn, *Appl. Phys. Lett.*, 1975, **27**, 103.

24 O. Kahn, *Molecular Magnetism*, VCH Publishers, 1993.

